Rev. Roum. Sci. Techn.– Électrotechn. et Énerg.
Vol. **67**, *2*, pp. 175–180, Bucarest, 2022

Automatique et ordinateurs

H∞ CONTROL-BASED ROBUST POWER SYSTEM STABILIZER FOR STABILITY ENHANCEMENT

ABDESLEM KHELLOUFI[1], BILAL SARI[1], SEIF EDDINE CHOUABA[2]

Keywords: Power system stabilizer; Robust control; H∞ approach; Single-machine system; Low-frequency oscillations.

A robust *H*∞ output feedback control approach is used to design power system stabilizers (PSS) for damping electrical power low-frequency oscillations over a wide range of operating conditions. Two *H*∞ control schemes have been employed in the Single-Machine connected to an infinite bus (SMIB) system. The proposed stabilizers offer robust stability against different unknown loads, considered an external disturbance. The simulation results show good performance and stability enhancement. The effectiveness of the proposed approach is demonstrated by a comparative study with three other approaches: conventional PSS and robust power system stabilizers based on quantitative feedback theory (QFT).

NOMENCLATURE

Δv	Speed deviation (p.u.)
Δv_{max}	Maximum speed deviation (p.u.)
δ	Power angle (rad)
δ_0	Initial power angle (rad)
ω	Rotor angular speed (rad/s)
ω_s	Synchronous rotor angular speed (rad/s)
θ	Power angle (deg)
D	Damping coefficient
E'_q	q-axis transient internal voltage (p.u.)
e_{d0}	Initial d-axis terminal voltage (p.u.)
E_{fd}	Rotor field voltage (p.u.)
e_{q0}	Initial q-axis terminal voltage (p.u.)
e_{t0}	Initial condition of terminal voltage (p.u.)
H	Inertia constant (s)
I_d, I_q	d and q-axis components of the generator stator current (p.u.)
I_g	Generator current (p.u.)
K_A	Automatic Voltage Regulator (AVR) gain
P, Q	Active and reactive powers (p.u.)
R_e, X_e	Line resistance and reactance (p.u.)
T'_{do}	d-axis transient open circuit time constant (s)
T_A	Automatic Voltage Regulator (AVR) time constant (s)
T_e	Electrical torque (p.u.)
T_m	Mechanical torque (p.u.)
V_∞	Infinite bus voltage (p.u.)
V_d, V_q	d and q-axis components of the terminal voltage (p.u.)
V_t	Terminal voltage (p.u.)
V_{ref}	Reference voltage (p.u.)
X'_d	d-axis transient reactance (p.u.)
X_d, X_q	d and q axis reactances (p.u.)

1. INTRODUCTION

Low-frequency electromechanical oscillations are a significant problem for power system stability. The range of these oscillations is between 0.01 and 3Hz. The instability of the power system can lead to blackouts. Among additional controllers used to improve low-frequency oscillations damping is power system stabilizers (PSS), which are used to produce a supplementary damping torque signal through the automatic voltage regulator (AVR) [1].

These low-frequency electromechanical oscillations are associated with the small-signal stability of a power system. They are divided into an inter-area mode, a torsional mode, and a local mode [2].

The conventional power system stabilizer (CPSS) works efficiently at the nominal operating point and its performance decreases if the operating point changes [3]. In this case, the conventional *PSS* does not warrant the robustness of a power system for various ranges of operating conditions. To solve the robustness problem, the robust control design could guarantee robust stability for different operating conditions where the system is subject to external disturbance or parametric uncertainties [4].

The conventional power system stabilizer design based on a lead-lag compensator is one of the traditional techniques widely implemented in industrial *AVR* [5]. Besides, several optimization algorithms have been used to damp power system oscillations, one cites genetic algorithm [6], bio-inspired algorithms [7], particle swarm optimization (PSO) [8], cuckoo search optimization (CSO) technique [9] used to tune the *PSS* two lead-lag blocks, farmland fertility algorithm (FFA) [10], hyper-spherical search (HSS) optimization algorithm [11]. Therefore, nonlinear control methods have been designed as sliding mode control [12], and the artificial intelligence-based training and tuning methods have been used to design a *PSS* as a deep reinforcement learning-based method [13]. Furthermore, robust control theories have been employed in the design of robust power system stabilizers [14]. In [15], a linear matrix inequalities (LMI) technique is used to synthesize a robust pole placement for a single machine and multi-machines power system. In [16], an *H*∞ feedback controller is applied to a non-linear dynamical model of a multi-machine power system.

In [17], the author used the μ-synthesis approach to design a coordinated control of *PSS* and additive High-voltage direct current (HVDC) damping controller in an

[1] DAC Laboratory, Electrical Engineering Department, University of Setif 1, 19000, Algeria, E-mail: Abdeslem.khelloufi@univ-setif.dz
[2] DAC Laboratory, University of Setif 1, Setif 19000, Algeria

ac/dc power system to attenuate intra-area mode oscillations.

Robust control techniques based on H_2 and H_∞ Norm have been developed in [3] using three weighting filters applied on a *SMIB*.

This paper proposes two H∞ control schemes to design robust PSS and apply them to the *SMIB* system. The first scheme uses two weighting filters and the other uses four weighting filters and considers the system robustness in the *PSS* synthesis phase. The effectiveness of the proposed technique is demonstrated by a comparison of the obtained simulation results with three other techniques.

This paper is organized as follows. Section 2 gives a description of the *SMIB* mathematical model. Section 3 explains the control problem formulation. Section 4 presents the proposed resolution and the chosen weighting filters used in the proposed design. Section 5 shows simulation results, in which a comparative study is carried out between the *QFT*-based power system stabilizers, a conventional *PSS* [4], and the proposed control strategies. Finally, Section 6 ends this paper and gives some concluding observations.

2. SYSTEM MODEL

The system used in this study is a Single Machine connected to Infinite Bus (SMIB) through an external reactance X_e and external resistance R_e as shown in Fig. 1.

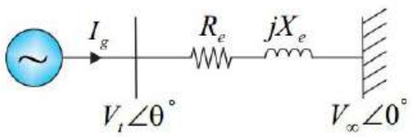

Fig. 1 – Diagram of *SMIB* system.

The model of the synchronous machine is described by the following equations:

$$\dot{\omega} = \frac{\omega_s}{2H}\left[T_m - \left(E_q^{'} I_q + \left(X_q - X_d^{'}\right) I_d I_q\right) - D\left(\omega - \omega_s\right)\right], \quad (1)$$

$$\dot{\delta} = \left(\omega - \omega_s\right), \quad (2)$$

$$\dot{E}_q^{'} = \frac{1}{T_{do}^{'}}\left(E_q^{'} + \left(X_d - X_d^{'}\right) I_d - E_{fd}\right), \quad (3)$$

$$\dot{E}_{fd}^{'} = \frac{1}{T_A}\left[-E_{fd} + K_A\left(V_{ref} - V_t\right)\right], \quad (4)$$

where all the model numerical values are given in the appendices. The *Heffron-Philips* model of the *SMIB* system [18] is used in the proposed design as shown in Fig. 2.

The following linearized state-space model will be considered for the H_∞ *PSS* control design:

$$\Delta\dot{x} = A\Delta x(t) + B_1\Delta w(t) + B_2\Delta u(t),$$
$$\Delta y(t) = C\Delta x(t), \quad (5)$$

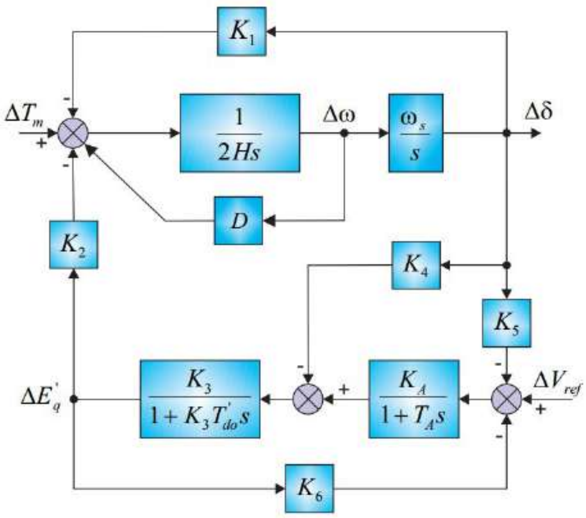

Fig. 2 – Scheme of Heffron-Phillips model.

where the matrices A, B, and C are defined as:

$$A = \begin{bmatrix} \frac{-1}{K_3 T_{do}^{'}} & \frac{-K_4}{T_{do}^{'}} & 0 & \frac{1}{T_{do}^{'}} \\ 0 & 0 & \omega_s & 0 \\ \frac{-K_2}{2H} & \frac{-K_1}{2H} & \frac{-D\omega_s}{2H} & 0 \\ \frac{-K_A K_6}{T_A} & \frac{-K_A K_5}{T_A} & 0 & \frac{-1}{T_A} \end{bmatrix}, \quad (6)$$

$$B = \left[B_1 \middle| B_2\right] = \begin{bmatrix} 0 & 0 & 0 \\ 0 & 0 & 0 \\ 0 & \frac{1}{2H} & 0 \\ \frac{K_A}{T_A} & 0 & \frac{K_A}{T_A} \end{bmatrix}, \quad (7)$$

$$C = \begin{bmatrix} 0 & 0 & 1 & 0 \end{bmatrix}, \quad (8)$$

where $\Delta x(t) = \left[\Delta E_q^{'} \quad \Delta\delta \quad \Delta v \quad \Delta E_{fd}\right]^T$ is the state vector, $\Delta w(t) = \left[\Delta V_{ref} \quad \Delta T_m\right]^T$ is the vector of the external inputs (external disturbances), the control signal (the output of the power system stabilizer) is The picture can't be displayed. and the system output signal is The picture can't be displayed.. The numerical values of the system parameters are calculated by the relationships given in the appendices.

3. CONTROL PROBLEM FORMULATION

Figure 3 illustrates the standard formulation of the problem, where $P(s)$ is a transfer matrix of the plant, $K(s)$ is the H_∞ *PSS*, w is the vector of the external inputs and disturbances, z is the vector of the outputs to be controlled, y is the measurement outputs and u is a control signal [19,20]. In this paper, the choice of the input/output of the standard problem is given by the external inputs w are the reference voltage variation ΔV_{ref} and the mechanical torque variation, ΔT_m. The measurement output y is the variation of the speed deviation Δv. The control signal u is the H_∞ (HPSS) output ΔV_{pss} and the external outputs z depend to two proposed designs and they will be given in the next section.

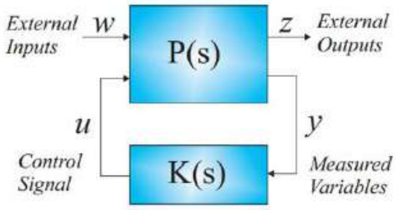

Fig. 3 – Standard control configuration.

The open-loop transfer matrix from $\begin{bmatrix} z \\ y \end{bmatrix}$ to $\begin{bmatrix} w \\ y \end{bmatrix}$ is:

$$\begin{bmatrix} z \\ y \end{bmatrix} = \begin{bmatrix} P_{11}(s) & P_{12}(s) \\ P_{21}(s) & P_{22}(s) \end{bmatrix} \begin{bmatrix} w \\ y \end{bmatrix}. \tag{9}$$

The linear fractional transformation (LFT) of the problem is given by:

$$T_{zw}(s) = P_{11}(s) + P_{12}(s)K(s)[I - P_{22}(s)K(s)]^{-1} P_{21}(s), \tag{10}$$

The H_∞ control problem is formulated as a minimization of the H_∞ norm γ such that:

$$\|T_{zw}(s)\|_\infty < \gamma. \tag{11}$$

The state space representation of the system can be given by the following equation:

$$\begin{bmatrix} \dot{x} \\ z \\ y \end{bmatrix} = \begin{bmatrix} A & B_1 & B_2 \\ C_1 & D_{11} & D_{12} \\ C_2 & D_{21} & D_{22} \end{bmatrix} \begin{bmatrix} x \\ w \\ u \end{bmatrix}, \tag{12}$$

where A is defined in (6) and

$$B_1 = \begin{bmatrix} 0 & 0 \\ 0 & 0 \\ 0 & \frac{1}{2H} \\ \frac{K_A}{T_A} & 0 \end{bmatrix}, \; B_2 = \begin{bmatrix} 0 \\ 0 \\ 0 \\ \frac{K_A}{T_A} \end{bmatrix}, \; D_{11} = \begin{bmatrix} 1 & 0 \\ 0 & 0 \end{bmatrix},$$

$$C_1 = \begin{bmatrix} -K_6 & -K_5 & 0 & 0 \\ 0 & 0 & 0 & 0 \end{bmatrix}, D_{12} = \begin{bmatrix} 0 \\ 1 \end{bmatrix},$$

$$C_2 = [0 \;\; 0 \;\; 1 \;\; 0], \; D_{21} = [0 \;\; 0], \; D_{22} = [0].$$

4. H∞ CONTROLLER RESOLUTION

4.1. CONTROLLER WITHOUT ROBUSTNESS WEIGHTING FILTER $W_3(s)$

To impose some dynamical performances in a H_∞ problem, it is necessary to include some weighting filters. In the first proposed design, two weighting filters $W_1(s)$ and $W_2(s)$ are included in the Plant as shown in Fig.4. In this case, the new considered external outputs are: z_1 and z_2, where z_1 is the measurement output $y(t)$ (speed deviation Δv) connected to the error weighting filter W_1 ($z_1 = W_1(s) \cdot y$) and z_2 is the control signal $u(t)$ (*PSS* voltage output ΔV_{pss}) connected to control weighting filter W_2 ($z_2 = W_2(s) \cdot u$).

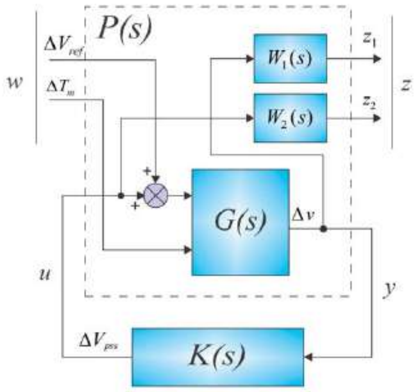

Fig. 4 – Filters augmentation of the system without using $W_3(s)$.

The choice of these weighting filters is an important step, an error weighting filter W_1 is chosen to limit the peak of the speed deviation Δv

$$W_1(s) = \frac{1}{\Delta v_{\max}}. \tag{13}$$

The control weighting filter $W_2(s)$ (given by the equation 14) is chosen to accelerate the convergence of the *HPSS* output ΔV_{pss} to zero and therefore, the settling time of speed deviation Δv will be reduced.

$$W_2(s) = \frac{w_b}{s + w_b \varepsilon}, \tag{14}$$

where w_b and ε are the tuning parameters. The following parameters values satisfy the design requirements for the nominal operating condition ($P = 0.8$ p.u., $Q = 0.4$ p.u. and $X_e = 0.2$p.u.): $\Delta v_{\max} = 10^{-3}$, $w_b = 62.5$ and $\varepsilon = 10^{-4}$.

To facilitate the *PSS* implementation, the obtained *HPSS* can be reformulated in the following form (like a conventional *PSS* structure with additional filter):

$$K(s) = \frac{K_s(s+T_1)(s+T_2)(s^2 + a_1 s + b_1)}{(s+T_3)(s+T_4)(s^2 + a_2 s + b_2)}. \tag{15}$$

The parameters numerical values of the obtained *HPSS1* controller are given in Table 1.

Table 1

HPSS1 parameters

$K_s = -2.12 \cdot 10^7$	$T_3 = 223.4$	$b_1 = 160.2$
$T_1 = -20.86$	$T_4 = 5 \cdot 10^{-7}$	$a_2 = 5657$
$T_2 = 6.25 \cdot 10^{-3}$	$a_1 = 23.65$	$b_2 = 9.23 \cdot 10^6$

Remark: it is noted that the order of the designed *HPSS1* is equal to the sum of the system order and the weighting filter order. With a cancellation of a zero and a pole, the proposed design leads to an *HPSS1* of order 4.

4.2. CONTROLLER WITH ROBUSTNESS WEIGHTING FILTER $W_3(s)$ AND VOLTAGE ERROR WEIGHTING FILTER $W_{dV}(s)$

In the second design proposed in this paper, four weighting filters are included in the Plant as shown in Fig.5. In this case, in addition to the external outputs z_1 and z_2 proposed in the previous design, two other outputs z_3 and z_4 are considered, where z_3 is the voltage error ($V_{dV} = \Delta V_{ref} - \Delta V_t$) connected to the weighting filter W_{dV} ($z_3 = W_{dV}(s)V_{dV}$) and z_4 is the terminal voltage ΔV_t connected to the robustness weighting filter W_3 ($z_4 = W_3(s)\Delta V_t$). The weighting filters are given in the following: $W_1(s) = 2.5 \cdot 10^5$, $W_2(s) = \dfrac{1}{0.1}$, $W_3(s) = \dfrac{600}{s+6}$, $W_4(s) = \dfrac{2 \cdot 10^4}{s + 0.002}$. The obtained *HPSS2* controller is designed to consider several operating conditions (P, Q, X_e) through the weighting filters, can be reformulated as follows:

$$K(s) = \frac{K_s(s+T_1)(s+T_2)(s+T_3)(s^2+a_1 s+b_1)}{(s+T_4)(s+T_5)(s+T_6)(s^2+a_2 s+b_2)}, \tag{16}$$

where its parameters are given in Table 2.

Table 2

HPSS2 Parameters

$K_s = 7.44 \cdot 10^6$	$T_4 = 787.20$	$a_1 = 26.13$
$T_1 = 6.00$	$T_5 = 14.08$	$b_1 = 197.40$
$T_2 = 4.03$	$T_6 = 6.00$	$a_2 = 188.00$
$T_3 = -0.01$	$T_7 = 5.06 \cdot 10^{-3}$	$b_2 = 1.70 \cdot 10^4$

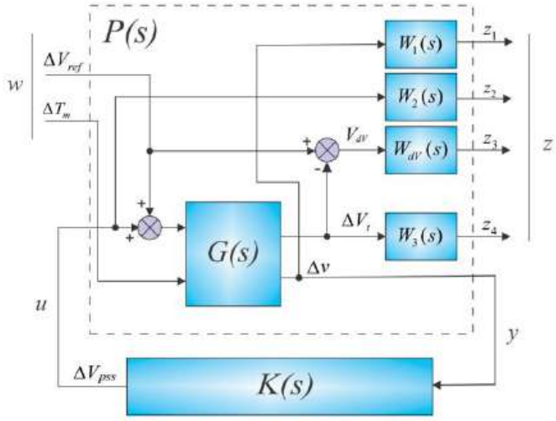

Fig. 5 – Filters augmentation of the system with using $W_3(s)$ and $W_{dV}(s)$.

5. **SIMULATION RESULTS**

To prove the robustness and effectiveness of the proposed H_∞ *PSS* controllers (called *HPSS* in the following figures), several studies have been performed on the SMIB system at different operating conditions, where the parameters of the system components are given in the Appendices. Furthermore, a comparative study is carried out with three methods: conventional *PSS* [5] (called *CPSS* in the following figures) and two other methods based on Quantitative Feedback Theory (simplex and Nonlinear programming methods) [4] (called in the following figures *QFT1-PSS* and *QFT2-PSS* respectively). Three different operating conditions have been considered with respect to the active power P, the reactive power Q, and the reactance of the transmission line X_e. A 5% step disturbance at the *AVR* voltage reference input is applied for the following three operating conditions:

- 1st test: $P = 0.8$ p.u., $Q = 0.4$ p.u. and $X_e = 0.2$ p.u.
- 2nd test: $P = 0.8$ p.u., $Q = 0.0$ p.u. and $X_e = 0.6$ p.u.
- 3rd test: $P = 1.0$ p.u., $Q = 0.5$ p.u. and $X_e = 0.7$ p.u.

The comparison of the simulation results obtained with conventional *PSS* (*CPSS*) and *QFT*-based *PSSs* (*QFT1-PSS* and *QFT2-PSS*) shows that the proposed *HPSS* stabilizers achieve better performances.

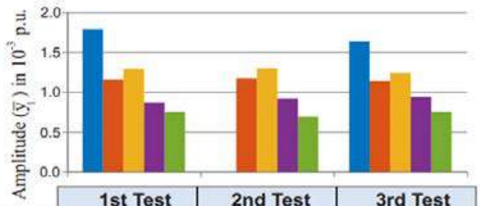

	1st Test	2nd Test	3rd Test
HPSS1	$0.87 \cdot 10^{-3}$	$0.92 \cdot 10^{-3}$	$0.94 \cdot 10^{-3}$
HPSS2	$0.75 \cdot 10^{-3}$	$0.69 \cdot 10^{-3}$	$0.75 \cdot 10^{-3}$
QFT1	$1.29 \cdot 10^{-3}$	$1.30 \cdot 10^{-3}$	$1.24 \cdot 10^{-3}$
QFT2	$1.16 \cdot 10^{-3}$	$1.17 \cdot 10^{-3}$	$1.14 \cdot 10^{-3}$
CPSS	$1.79 \cdot 10^{-3}$	Unstable	$1.64 \cdot 10^{-3}$

Fig. 6 – Comparison of the first oscillation amplitude of proposed *PSSs* conventional *PSS* and *QFT*-based *PSSs*.

Figures 6, 7, and 8 show a quantitative comparison of the proposed *PSSs* with conventional *PSS* and *QFT*-based *PSSs,* where, the parameter $\bar{y}_1$ represents the first oscillation amplitude of the system response, $\bar{y}_2$ is the amplitude of the second oscillation and t_s is the settling time for $|y| < 0.0001$, where y is the speed variation.

Figures 9, 10, and 11 present respectively the simulation results of rotor angular speed variation Δv and the power system stabilizer control signal ΔV_{pss} for the 1st, 2nd, and 3rd tests. As can be observed from these figures, the first oscillation amplitudes of the proposed *PSSs* (*HPSS*) are less than the other controllers in all the performed tests.

The *QFT*-based *PSSs* have two other oscillations before the stability in the 2nd and the 3rd tests, whereas the conventional *PSS* cannot stabilize the system in the 2nd test and it has many oscillations in the 3rd test, while the first proposed *PSS* (*HPSS1*) has only one oscillation in all the performed tests. It is noted that the first oscillation of the second proposed *PSS* (*HPSS2*) is smaller than all the other *PSS*. Furthermore, the amplitude of its second oscillation is better than *QFT*-based *PSSs*. The settling time of the first proposed *PSS* is less than half the value of the others in the 2nd and the 3rd tests.

The second proposed design has a good settling time in the 2nd and the 3rd tests compared to *QFT*-based *PSSs* and conventional *PSS*. At the end, it is noted that the control signal of the proposed *HPSS* is in the range $-0.1 < V_{pss} < 0.1$ in all the performed tests as recommended by [5].

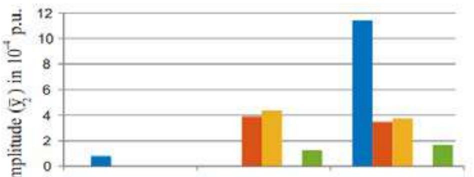

	1st Test	2nd Test	3rd Test
HPSS1	0.00	0.00	0.00
HPSS2	0.00	$1.20\cdot10^{-4}$	$1.62\cdot10^{-4}$
QFT1	0.00	$4.32\cdot10^{-4}$	$3.72\cdot10^{-4}$
QFT2	0.00	$3.87\cdot10^{-4}$	$3.45\cdot10^{-4}$
CPSS	$0.75\cdot10^{-4}$	Unstable	$11.41\cdot10^{-4}$

Fig. 7 – Comparison of the second oscillation amplitude of proposed *PSSs* conventional *PSS* and *QFT*-based *PSSs*.

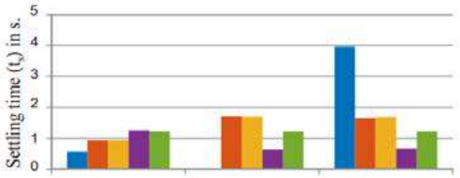

	1st Test	2nd Test	3rd Test
HPSS1	1.26	**0.64**	**0.67**
HPSS2	1.23	1.23	1.23
QFT1	0.94	1.69	1.68
QFT2	0.94	1.70	1.66
CPSS	**0.57**	Unstable	3.96

Fig. 8 – Comparison of the settling time obtained with proposed *PSSs, QFT1* and *QFT2 PSSs* and a conventional *PSS*.

6. CONCLUSIONS

In this paper, a robust power system stabilizer using H_∞ control approach is applied to a Single Machine connected to an Infinite Bus (SMIB) system. The main objective is to enhance the stability and the robustness of the *SMIB* against different unknown loads, external disturbances (Steps in the reference voltage or in the applied torque) and the variation of the external reactance X_e. The first proposed *HPSS1* has a simple architecture, simple weighting filters, and good performance. The second proposed design *HPSS2* has good robustness and good performance compared to conventional *PSS* and *QFT-PSSs*.

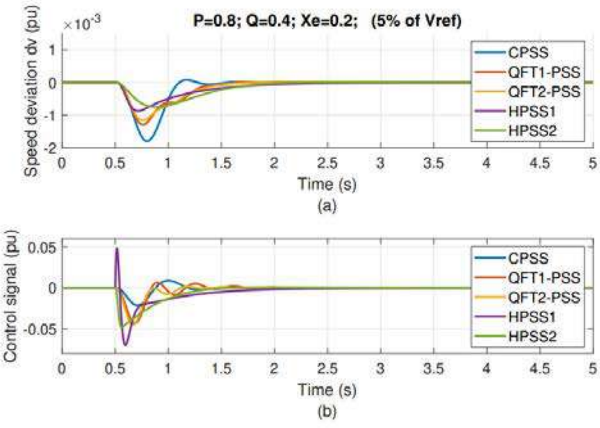

Fig. 9 – *SMIB* response to a 5% step disturbance at the voltage reference input, (1st test: $P = 0.8$, $Q = 0.4$ and $X_e = 0.2$).

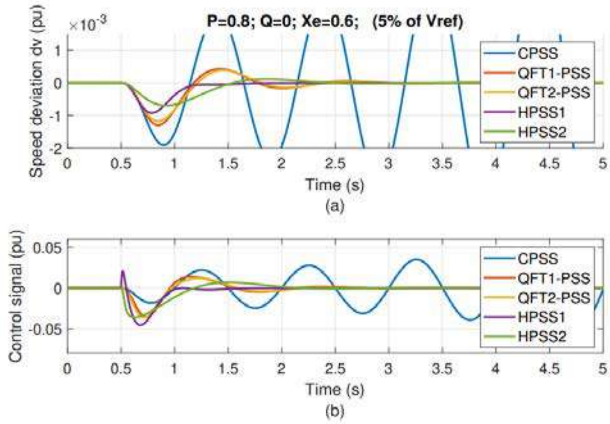

Fig. 10 – *SMIB* response to a 5% step disturbance at the voltage reference input, (2nd test: $P = 0.8$, $Q = 0.0$ and $X_e = 0.6$).

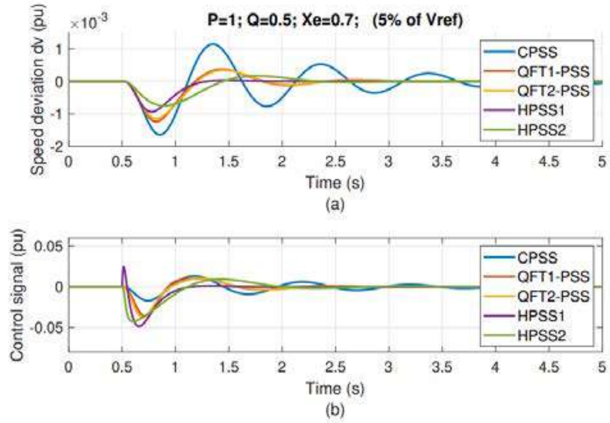

Fig. 11 – *SMIB* response to a 5% step disturbance at the voltage reference input, (3rd test: $P = 1.0$, $Q = 0.5$ and $X_e = 0.7$).

The simulation results confirm the great benefit of a robust H_∞ *PSS* output feedback controller compared to the *QFT*-based *PSSs* regarding the time response, the speed deviation dynamic, and the disturbance rejection. As a perspective, the proposed design will be applied to a multi-machine system to damp inter-area oscillations.

APPENDIX

A. THE SMIB EQUATIONS

In this section, the relationships for a *SMIB* are defined as in [21]. The expression used to calculate the system constants K_1 to K_6 are defined as follows:

$$K_1 = \frac{X_q - X_d^{'}}{X_e + X_d^{'}} I_{q0} V_\infty \sin\delta_0 + \frac{V_{q0} V_\infty \cos\delta_0}{X_e + X_q},$$

$$K_2 = \frac{V_\infty}{X_e + X_d^{'}} \sin\delta_0,\ K_3 = \frac{X_d^{'} + X_e}{X_d + X_e},$$

$$K_4 = \frac{X_d - X_d^{'}}{X_e + X_d^{'}} V_\infty \sin\delta_0,$$

$$K_5 = \frac{X_q}{X_e + X_q}\frac{e_{d0}}{e_{t0}} V_\infty \cos\delta_0 - \frac{X_d^{'}}{X_e + X_d^{'}}\frac{e_{q0}}{e_{t0}} V_\infty \sin\delta_0,$$

$$K_6 = \frac{X_e}{X_e + X_d^{'}}\frac{e_{q0}}{e_{t0}}$$

B. THE SMIB DATA

The parameters in per unit of the *SMIB* [4] presented in Fig.1 are given in Table B.3.

Table B.3

The system data

$X_d = 2.0 p.u.$	$T'_{do} = 4.18 s$	$V_\infty = 1 p.u.$
$X_q = 1.91 p.u.$	$K_A = 50 p.u.$	$H = 3.25 s$
$X'_d = 0.244 p.u.$	$T_A = 0.05 s$	$\omega_s = 314 rad/s$

C. THE CONVENTIONAL PSS AND QFT-PSSS DATA

The transfer function of the *CPSS* is given as follows:

$$K_0(s) = K_s \frac{(s+T_1)^2}{(s+T_2)^2},$$

where K_s, T_1 and T_2 are respectively the *PSS* gain and its parameters. The CPSS and QFT- PSSs parameters obtained by [4] are given in the Table C.5.

Table C.5

CPSS, QFT1 and QFT2 Parameters, [4]

Controller Parameters	Design Method		
	QFT1	QFT2	CPSS
K_s	13.88	16.22	5.5
T_1	0.1785	0.1542	0.1732
T_2	0.0614	0.0440	0.0577

Received on 19 May 2021.

REFERENCES

1. A. Sallam, O.P. Malik, *Power system stability: modelling, analysis and control*, The Institution of Engineering and Technology (2015).
2. P. Kundur, N. J. Balu, M. G. Lauby, *Power system stability and control*, McGraw-hill New York (1994).
3. A. Sil, T. Gangopadhyay, S. Paul, A. Maitra, *Design of robust power system stabilizer using H∞ mixed sensitivity technique*, 2009 International Conference on Power Systems (IEEE), Kharagpur, India (2009).
4. P. Shrikant Rao, Indraneel Sen, *Robust tuning of power system stabilizers using QFT*, IEEE transactions on control systems technology, **7**, *4*, pp. 478-486 (1999).
5. *IEEE Recommended Practice for Excitation System Models for Power System Stability Studies*, IEEE Std 421.5-2016 (Revision of IEEE Std 421.5-2005, pp. 1–207 (2016).
6. H. Labdelaoui, F. Boudjema, D. Boukhetala, *Multiobjective optimal design of dual-input power system stabilizer using genetic algorithms,* Rev. Roum. Sci. Techn. – Électrotechn. Et Énerg., **62**, *1*, pp. 93–97 (2017).
7. E. L. Miotto, P. B. de Araujo, E. de Vargas Fortes, B. R. Gamino, L. F. B.Martins, *Coordinated tuning of the parameters of PSS and POD controllers using bioinspired algorithms*, IEEE Transactions on Industry Applications **54**, *4*, pp. 3845–3857 (2018).
8. G. Shahgholian, A. Mohavedi, *Coordinated design of thyristor-controlled series capacitor and power system stabilizer controllers using velocity update relaxation particle swarm optimization for two machine power system stability*, Rev. Roum. Sci. Techn. – Électrotechn. et Énerg., **59**, pp. 291–301 (2014).
9. S. Abd Elazim, E. Ali, *Optimal power system stabilizers design via cuckoo search algorithm*, International Journal of Electrical Power & Energy Systems **75**, pp. 99–107 (2016).
10. A.N. Sabo, I. Abdul Wahab, M.L. Othman, M.Z.A. Mohd Jaffar, H. Beiranvand, *Optimal design of power system stabilizer for multi-machine power system using farmland fertility algorithm*, International Transactions on Electrical Energy Systems (2020).
11. M. Rahmatian, S. Seyedtabaii, *Multi-machine optimal power system stabilizers design based on system stability and nonlinearity indices using hyper-spherical search method*, International Journal of Electrical Power & Energy Systems **105**, pp. 729–740 (2019).
12. A. Mourad, G. Keltoum, *Power system stabilizer based on terminal sliding mode control,* Rev. Roum. Sci. Techn. – Électrotechn. et Énerg., **62**, *1*, pp. 98–102 (2017).
13. G. Zhang, W. Hu, D. Cao, Q. Huang, J. Yi, Z. Chen, F. Blaabjerg, *Deep reinforcement learning-based approach for proportional resonance power system stabilizer to prevent ultra-low-frequency oscillations*, IEEE Transactions on Smart Grid, **11**, *6*, pp. 5260–5272 (2020).
14. S. Chen, O. Malik, *H∞ optimization-based power system stabilizer design*, IEEE Proceedings-Generation, Transmission and Distribution, **142**, *2*, pp. 179–184 (1995).
15. P.S. Rao, I. Sen, *Robust pole placement stabilizer design using linear matrix inequalities*, IEEE Transactions on Power Systems, **15**, *1*, pp. 313–319 (2000).
16. G. Rigatos, P. Siano, A. Melkikh, N. Zervos, *A nonlinear H-infinity control approach to stabilization of distributed synchronous generators*, IEEE Systems Journal, **12**, *3*, pp. 2654–2663 (2017).
17. R. Chen, Y. Zhang, *Coordinated control of power system stabilizers and HVDC damping controller using decentralized μ-synthesis*, 2006 International Conference on Power System Technology (IEEE), Chongqing, China (2006).
18. P. Sauer, M. Pai, J. Chow, *Power System Dynamics and Stability: With Synchrophasor Measurement and Power System Toolbox*, Wiley & Sons, Inc. (2017).
19. S. Gerwig, B. Sari, F. Garin, C. Canudas-de-Wit, *Controller for Hydroelectric Group*, USA Patent No. US 10,505,480 B2, 2019.
20. B. Sari, M. F. Benkhoris, J.C. Le Claire, B. Rabhi, *Robust H∞ output feedback control design applied to uninterruptible power supplies,* 2012 International Symposium on Industrial Electronics (IEEE), Hangzhou, China (2012).
21. F.P. Demello, C. Concordia, *Concepts of synchronous machine stability as affected by excitation control*, IEEE Transactions on power apparatus and systems, **88**, *4*, pp. 316–329 (1969).